Draft of November 20, 2007

Shock heating in the nearby radio galaxy NGC 3801

J.H. Croston[1], R.P. Kraft[2], M.J. Hardcastle[1]

ABSTRACT

We report the *Chandra* detection of shock-heated shells of hot gas surrounding the radio lobes of the nearby ($D_L \sim 53$ Mpc) low-power radio galaxy NGC 3801. The shells have temperatures of 1 keV and 0.7 keV, compared to an ISM temperature of 0.23 keV. The estimated expansion speed of the shells is ~ 850 km s^{-1}, corresponding to a Mach number of ~ 4. This is the second X-ray detection of strong shocks produced by a low-power radio galaxy, and allows us to measure directly the contribution of shock heating to the radio galaxy's total energetic input to the ISM. We show that the gas properties of the shells and surrounding ISM are consistent with the Rankine-Hugoniot shock jump conditions. We estimate the energy stored in the hot gas shells (thermal + kinetic energy) to be 1.7×10^{56} ergs, which is equivalent to the thermal energy of the ISM within ~ 11 kpc of the galaxy centre, and a factor of ~ 25 larger than the inferred $P\mathrm{d}V$ work required to inflate the lobe cavities, indicating that energy transfer from the AGN to its environment is dominated by shock heating during this stage of radio-source evolution. Our results provide direct evidence that shock heating in the early supersonic phase of FRI radio-source expansion can have important long-term effects on the properties of the host galaxy ISM. Finally, we discuss the merger history of NGC 3801, the fuelling of its AGN and the role of this type of system in feedback models.

Subject headings: galaxies: active – X-rays: galaxies – X-rays: quasars – radiation mechanisms: non-thermal

[1]School of Physics, Astronomy and Mathematics, University of Hertfordshire, College Lane, Hatfield AL10 9AB, UK

[2]Harvard-Smithsonian Center for Astrophysics, 60 Garden Street, Cambridge, MA 02138, USA

1. Introduction

Shock heating by radio galaxies is thought to be an important means of transferring energy from active galactic nuclei to their environments, but direct evidence for this process has been difficult to find. The first example of a shock associated with expanding radio-galaxy lobes was found in the nearest low-power (FRI) radio galaxy, Centaurus A (Kraft et al. 2003), and this remains the only case to date in which a high Mach number shock can be seen in direct contact with a radio lobe. Other examples of shocks have been found in clusters, where they are often detached from the radio lobes and always considerably weaker (e.g. M87: Forman et al. 2005, Cygnus A: Wilson et al. 2006; Hydra A: Nulsen et al. 2006); these results confirm that energy input via shocks is an important mechanism for AGN feedback on scales ranging from individual galaxies to galaxy clusters. It is therefore essential to be able to constrain the physical properties of radio-lobe shocks, and to understand in what circumstances they occur, so as to be able to measure the total energy contribution from radio galaxies to their environments.

The detection of shocked gas in the low-power (FRI) radio galaxy Centaurus A (Kraft et al. 2003), suggests that the early stages of radio-source expansion will have a dramatic effect on the host galaxy ISM. Well-studied, large FRI sources are not thought to be overpressured (e.g. Croston et al. 2003); however, it is likely that all radio sources go through an early overpressured phase of supersonic expansion, producing shocks, before achieving pressure balance (e.g Heinz et al. 1998). While the highly supersonic phase of expansion must last for only a small fraction of the source's lifetime, the impact on the surrounding gas properties of the shock heating it produces may be dramatic, since the energy input from such a source is a significant fraction of the gravitational energy of the gas: in the case of Cen A, the shock-heated gas has a thermal energy of 4.2×10^{55} ergs, which is a few tens of percent of that of the ISM (and its kinetic energy is significantly higher – see Kraft et al. (2003)). Low-power FRIs similar to Cen A are expected to be relatively common, and so the shock detection in Cen A leads to a prediction that many elliptical galaxies experience the effects of shock heating by supersonically expanding radio lobes. It is therefore essential to establish whether the shock conditions observed in Cen A, which do not agree with standard predictions, are likely to be typical of the effects of young FRI sources on their environments.

In this paper we report the *Chandra* detection of shocked gas shells surrounding the radio lobes of NGC 3801: this is the second such detection in a nearby radio galaxy. NGC 3801 is a nearby ($z = 0.0113$), isolated E/S0 galaxy, which hosts a small double-lobed radio source of similar morphology to Cen A. Optically, NGC 3801 is disturbed, with a prominent dust lane and secondary dust features, as shown in HST WFPC2 images (Verdoes Kleijn et al. 1999). Recent millimeter-wave observations with BIMA (Das et al. 2005) have revealed the presence of a central rotating molecular gas ring or disk, as well as a gas clump likely to be infalling merger-related

material that may be interacting with the radio jet. These results indicate that NGC 3801 has recently undergone a merger; our *Chandra* data therefore also provide an opportunity to investigate the relationship between merger activity, AGN fuelling and feedback via radio outbursts. Since small FRI sources like Cen A and NGC 3801 will be undetectable in the radio beyond $z \sim 0.04$ with the sensitivity of current instruments, these sources provide one of the few means of obtaining more information about the heating and compression of gas in more distant massive elliptical galaxies, where such radio sources are likely to be present but undetectable.

Throughout this paper, we adopt a cosmology with $H_0 = 70$ km s^{-1} Mpc^{-1}, $\Omega_M = 0.3$ and $\Omega_\Lambda = 0.7$. We adopt a luminosity distance fot NGC 3801 of 52.6 Mpc, obtained by correcting the heliocentric velocity of 3317 ks s^{-1} (Lu et al. 1993) to the CMB frame of reference, which gives an angular scale of 1 arcsec = 0.25 kpc at the distance of NGC 3801.

2. Data analysis

2.1. Chandra

We observed NGC 3801 with *Chandra* for 60 ks on 2006 April 6. The observation was taken in VFAINT mode to minimize the background level. The data were reprocessed from the level 1 events file with CIAO 3.3 and CALDB 3.2, including VFAINT cleaning. The latest gain files were applied and the 0.5-pixel randomization removed using standard techniques detailed in the CIAO on-line documentation[1]. In addition to applying the standard good time intervals we carried out GTI filtering using the *analyze_ltcrv* script, which reduced the total exposure time to 58,886 s.

We produced a 0.5 – 2 keV filtered image to examine the X-ray emission associated with the radio galaxy, presented in Fig. 1. X-ray emission is detected from the core of NGC 3801, from regions surrounding the two radio lobes, indicated in Fig. 1, and extended emission from the galaxy atmosphere is also detected. Fig. 2 shows a Gaussian smoothed image with radio contours overlaid (see below) emphasizing the lobe-related X-ray structure.

We extracted spectra from the core, the two lobes and the galaxy halo using the *specextract* script, which also builds the appropriate response files. Extraction regions are shown in Fig 3. Local background regions adjacent to or surrounding the source extraction regions were used. Spectra were grouped to 20 counts per bin after background subtraction prior to spectral fitting, which was carried out using XSPEC. We assumed a fixed Galactic absorption of $N_H = 2.3 \times 10^{20}$ cm^{-2} (Dickey & Lockman 1990) in all of our spectral fitting.

[1]http://asc.harvard.edu/ciao/

We also extracted a radial surface brightness profile for NGC 3801 to constrain the X-ray emission from the ISM, masking out the radio lobe regions and point sources, and using an outer annulus (between 74 and 123 arcsec) as a local background. The profile was extracted in the 0.5 – 2 keV energy range, where the contribution from the nuclear point source is negligible, so that the profile could be fitted by a β model convolved with the *Chandra* PSF, as parametrized by Worrall et al. (2001). Further analysis of the radial profile is described in Section 3.2. The background-subtracted radial profile is shown in Fig. 5.

2.2. Radio data

We observed NGC 3801 at 1.4 GHz and 4.9 GHz with the VLA on 2006 February 17 in A configuration, on 2006 June 27 in B configuration, and on 2006 November 26 to supplement existing archival data. The data were calibrated in the standard manner using AIPS. The *clean* algorithm was used to map the data for each frequency at each configuration, and in each case self-calibration was carried out to convergence using the clean model components. The final 1.4-GHz map was obtained by first combining our A-configuration data with an an earlier snapshot observation (AB920) in the same configuration to improve our *uv* coverage. The archive data were independently calibrated, and then the final *clean* model obtained from the new data was used to calibrate the archive dataset, prior to combining the *uv* data of the two observations using *dbcon*. The 1.4-GHz B-configuration data were then calibrated using the best A-configuration model, before being combined with the A-configuration data with appropriate weighting, using *dbcon*. A final map, shown in Fig. 2, was then produced from the combined data. The 4.9-GHz data were reduced similarly, with the C-configuration data first calibrated using the best B-configuration model before they were combined. The final combined B and C configuration map at 4.9-GHz has resolution matched to the combined A and B configuration map at 1.4-GHz, enabling spectral analysis to be carried out as discussed in Section 4.

3. Results

3.1. Radio lobe related emission

Although, the edge-brightned shell morphology of the lobe-related emission immediately suggests a hot gas origin, we initially fitted the spectra for the east and west lobe-related X-ray emission with single power-law and *mekal* models with the aim of distinguishing between a thermal and non-thermal origin. In neither case could a single power-law model provide an acceptable fit to the data. We calculate that the predicted X-ray flux from lobe inverse-Compton scattering of CMB

and synchrotron photons (e.g. Croston et al. 2005), based on the 1.4-GHz radio flux and assuming equipartition of energy density in magnetic fields and particles, is at least two orders of magnitude below that observed, so that we would not expect to see significant emission from these processes.

A good fit was obtained for the west lobe region with a *mekal* model having $kT = 1.0^{+0.4}_{-0.3}$ keV, assuming $Z = 0.3$ solar, giving $\chi^2 = 2.5$ for 2 d.o.f. The unabsorbed 0.4 - 2 keV flux from this component is $6.0^{+2.1}_{-1.5} \times 10^{-15}$ ergs cm^{-2} s^{-1}. For the eastern lobe we obtained a good fit ($\chi^2 = 5.6$ for 3 d.o.f.) with $kT = 0.71^{+0.09}_{-0.04}$ keV, giving an unabsorbed 0.4 - 2.0 keV flux of $(6.9 \pm 0.8) \times 10^{-15}$ ergs cm^{-2}. We carried out a free abundance fit for the west lobe, which did not significantly alter the measured temperature, and for the east lobe (which had too few bins for a similar test) we verified that varying the abundance between 0.28 (the lowest acceptable value) and 0.5 solar did not significantly affect the temperature, though in both cases the *mekal* normalization is affected (we discuss the effect of this uncertainty on the inferred gas density in Section 5.1). We also compared a range of background regions, including a large off source region, and regions on either side of the radio lobes, none of which affected the temperature determination for each lobe. Finally, we tested a combined power-law + mekal model for the west lobe, but obtained a very low power-law normalization and no significant change in temperature or temperature uncertainty. As stated above, there is no plausible physical origin for non-thermal X-ray emission of this strength associated with the radio lobes, and so we do not consider non-thermal models further.

If the hot gas is due to shocks, it is likely that the shells will have temperature structure, so that a single temperature *mekal* model is not ideal. In addition, the dust lane structure of the host galaxy could lead to variable absorption across the eastern shell. Unfortunately the photon statistics do not allow us to test for either of these scenarios and so in the discussion that follows we adopt the physical parameters obtained from the single temperature *mekal* fits. Our adopted spectral models for the lobe-related X-ray emission are shown in Fig. 4.

3.2. Interstellar medium and X-ray binary population

We used surface brightness profile analysis to investigate the extended emission from the X-ray halo of NGC 3801, using the 0.4 – 1 keV energy range and masking point sources to minimize any contamination from the resolved X-ray binary population in this galaxy. Extended emission is detected to a radius of $\sim$ 75 arcsec, which corresponds to $\sim$ 17 kpc. As the contribution from the central AGN in this energy range is negligible due to its heavy absorption, we simply fitted a β model convolved with the *Chandra* PSF using the model of Worrall et al. (2001). We obtained best-fitting values of $\beta = 0.45$ and $r_c = 7$ arcsec ; however, both the slope and core radius are poorly constrained due to the small numbers of counts. The profile and best-fitting model are shown in Fig. 5. The extent of the detected gas halo is comparable to the extent of

stellar light detected in the ground-based observations of Peletier et al. (1990), who calculated an effective radius of 11.1 kpc (transformed to our luminosity distance) based on the measurements of Burstein et al. (1987); however, the R-band surface brightness profile of Peletier et al. (1990) shows that the stellar distribution is considerably steeper than that of the hot gas.

We then extracted a spectrum for the region sampled by the radial profile (excluding the nucleus and lobe regions). A single *mekal* model resulted in an implausibly high temperature; however, there is likely to be a significant contribution from the unresolved X-ray binary population and so we fitted a model consisting of a *mekal* plus flat ($\Gamma = 1.0$) power-law to account for this component. A best-fitting temperature of $0.23^{+0.21}_{-0.09}$ keV was obtained (for fixed abundance of 0.4 solar, the measured value for Centaurus A, Kraft et al. 2003) resulting in a value of $\chi^2 = 3.8$ for 4 d.o.f. Fig. 6 shows the ISM spectrum with this best-fitting model. The temperature is not sensitive to abundance; however, the mekal normalisation varies by a factor of ~ 8 if the abundance is varied between 0.l and 1.0 times solar. We carried out simulations using the *fakeit* command in XSPEC, which demonstrated that we can obtain an unbiased estimate of the temperature for a value of 0.23 keV in the abundance range 0.1 to 1.0 times solar, with a 90 percent confidence range similar to the quoted uncertainties for an abundance of 0.4 times solar. Our fitted temperature is also in reasonable agreement with that inferred from the galaxy velocity dispersion (see Section 5.3). We measured an unabsorbed 0.4 - 7.0 keV flux of $4^{+5}_{-2} \times 10^{-15}$ ergs cm^{-2} s^{-1} from the thermal component, and a 1-keV flux density of 1.3 ± 0.5 nJy from the PL component. Modelling the hard component with a thermal bremsstrahlung component of $kT = 5-10$ keV, as might be expected for a population of low-mass X-ray binaries, does not significantly affect the best-fitting temperature or the luminosity of the *mekal* component. We determined the bolometric X-ray luminosity of the ISM, by integrating the best-fitting β model and using the best-fitting thermal model to convert from the total number of counts, to be $\sim 2 \times 10^{40}$ ergs s^{-1}. Since NGC 3801 has $M_B = -21.33$ (Peletier et al. 1990), this puts it in the middle of the L_X/L_{bol} distribution for elliptical galaxies, as studied by O'Sullivan et al. (1990). For an abundance of 0.4 times solar, the central density of the gas is 3×10^{-2} cm^{-3} (ranging from $2.5 \times 10^{-2} - 6 \times 10^{-2}$ cm^{-3} for abundances ranging from 0.1 to 1.0 times solar). We note that the radial distribution of the gas may differ somewhat from the beta model fitted above, since emission from X-ray binaries contributes ~ 40 percent of the flux in the energy range used; however, our X-ray surface brightness profile is much flatter than the stellar distribution (Peletier et al. 1990), so that it is likely to be dominated by the gas emission. Any systematic effect of the X-ray binary contribution must be to reduce the gas density at the radii of interest discussed further in Section 5.1. The unabsorbed 0.4 - 7 keV luminosity of the unresolved X-ray binary component is $\sim 7 \times 10^{39}$ erg s^{-1}, which is comparable to the total X-ray binary luminosity measured by Kraft et al. (2001) for Centaurus A.

There are several bright point sources within the D_{25} radius of the galaxy. To determine if any of these are likely to be ultra-luminous X-ray binaries (ULXs) related to NGC 3801, we

determined the positions and fluxes of the sources using the CIAO tool *wavdetect*. The brightest source contains 28 counts in the 0.5-2.0 keV band. To convert count rate to luminosity, we assume a 5 keV bremsstrahlung spectrum with Galactic absorption. A count rate of 10^{-3} cts s^{-1} in the 0.5-2.0 keV band corresponds to a flux of 6.3×10^{-15} ergs cm^{-2} s^{-1} in the 0.1-10.0 keV band (unabsorbed). The observed rate from the brightest source corresponds to a luminosity of $1.4{\times}10^{39}$ ergs s^{-1}. Based on the log(N)-log(S) relation of Tozzi et al. (2001), we expect $\sim$0.5 background AGN of this flux or higher within the D_{25} radius. There are eight other sources detected in the D_{25} radius with fluxes a factor of 3 to 7 lower than the brightest source. The X-ray luminosity of the brightest source does not qualify it as a ULX if it is related to NGC 3801, and there is a significant probability that it is an unrelated background AGN. Some of the less luminous sources are likely to be LMXBs related to the host galaxy at the high end of the luminosity function, none of which are ULXs. We conclude that none of the point sources are ULXs.

3.3. Core

The nuclear spectrum of NGC 3801 was poorly fitted with a single power-law model with Galactic absorption ($\chi^2/n > 2$): extremely prominent residuals are present at hard energies. We therefore added a second model component consisting of a heavily absorbed power law, which resulted in a good fit. A similar two power-law model was found to provide the best description of the nuclear spectrum of Centaurus A (e.g. Evans et al. 2004), and is commonly used to fit spectra of narrow-line radio galaxies.

The power-law index of the unabsorbed component is poorly constrained, and so we fixed its value at $\Gamma = 2$ (a typical value for unabsorbed power law components in FRI radio galaxies, e.g. Evans et al. 2006). The best fitting values of Γ and N_H for the second component were $0.6^{+0.4}_{-0.5}$ and $3.1^{+2.6}_{-1.6} \times 10^{22}$ cm^{-2}, respectively, giving $\chi^2 = 1.4$ for 5 d.o.f. We then fixed the second power-law index at the more physically plausible value of 1.5 (e.g. Evans et al. 2006; Hardcastle et al. 2006), which gave a best-fitting value of $N_H = 6.4^{+1.3}_{-1.1} \times 10^{22}$ cm^{-2} and $\chi^2 = 2.2$ for 6 d.o.f. This best-fitting model is shown in Fig. 8. The unabsorbed 1-keV flux densities in this model were 0.3 ± 0.1 nJy and 16 ± 2 nJy for the first and second power-law components, respectively, corresponding to an unabsorbed bolometric luminosity from the obscured component of 3×10^{41} ergs s^{-1}. The 5-GHz flux density of the core is 3.5 mJy, which means that the primary (unabsorbed) power law component lies close to the radio-X-ray core correlation for components with low intrinsic absorption reported by Evans et al. (2006), whereas the second (absorbed) power law lies significantly above the correlation, as is generally the case for heavily absorbed components. We therefore interpret the primary power law as jet-related in origin, and the second, heavily absorbed power law as having an accretion-related origin.

We used archive HST data (taken using the F555W and F814W filters on WFPC2) to measure the extinction from the central dust lane, which was converted to $E(B-V)$ and subsequently column density of neutral hydrogen using the relations of Zombeck (1990). We obtained a value of $N_H \sim 2 \times 10^{21}$ cm^{-2}, which is significantly lower than the column density obtained from our spectral fit, so that we conclude that, in addition to the absorption from the dust lane, the NGC 3801 must contain a substantial quantity of absorbing material instrinsic to the nucleus. Heavily absorbed nuclear spectra are not usually found in FRI radio galaxies (e.g. Evans et al. 2005); but Centaurus A is an exception, and it would appear that NGC 3801 is a second example of an FRI radio galaxy with a nucleus having high intrinsic absorption. We discuss the implications of this result further in Section 7.

4. Radio source age

We can use our two-frequency radio data to give us some constraints on the age of the radio source. The two-point spectral indices between 1.4 and 4.9 GHz in the outer regions of the source are only marginally steeper than those in the inner regions, as expected if the radio source is young. We fitted a Jaffe & Perola (1973) aged electron spectrum to the radio data in the outer regions of the source, assuming a constant ageing magnetic field of 2 nT (the mean equipartition field in the lobes). The main uncertainty in this model is the value of the low-frequency electron energy index (the 'injection index'). Young et al. (2005) have recently argued that in normal FRI sources the low-energy electron energy index tends to be close to 2.1 ($\alpha = 0.55$, where we define α in the sense that $S \propto \nu^{-\alpha}$). If we adopt this injection index then the spectral index in the steepest part of the lobe ($\alpha \approx 0.69$) corresponds to a source age of 2.4×10^6 years. If the injection index were steeper, the age would be reduced: for example, for an injection index corresponding to $\alpha = 0.65$, which is the flattest spectrum we observe in the jets, we fit an age of 8×10^5 years. It is probably reasonable to treat the age of 2.4×10^6 years as an upper limit. This value is in good agreement with the age we obtain from source dynamical arguments in Section 5.2.

5. Discussion

5.1. Physical properties of the gas shells, ISM and radio lobes

The spectral analysis presented in Section 3.1 revealed that the lobe-related thermal emission is significantly hotter than the surrounding ISM gas for both lobes. In this section we therefore investigate further the plausibility of a model in which we are observing shock-heated shells of gas around the radio lobes of NGC 3801.

We calculated the density and pressure of the gas in each shell region by assuming a spherical shell of gas with an outer radius defined by the outer edge of the detected X-ray emission ($R_{out} = 8$ arcsec for both lobes). We assume that the radio source is close to the plane of the sky, as suggested by Das et al. (2005) based on the two-sidedness of the jet and the orientation of the nuclear disk, and so we used projected distances to calculate the shell volume (if the source were at 45 degrees to the angle of sight, we would be underestimating the shell volumes by roughly a factor of 2). It is difficult to estimate the thickness of the shells accurately, because the photon statistics are poor, and so we chose conservative upper and lower limits based on the apparent thickness of the emission in the *Chandra* data (corresponding to a projected distance of ~ 500 pc), and the modelled thickness obtained for the shell in Centaurus A where the data quality is sufficient to allow a more accurate determination (corresponding to ~ 200 pc). The gas densities and pressures in the shells were then determined from the best-fitting *mekal* models for each lobe, and are given in Table 1 as a range based on the two volume estimates. The uncertainty due to the volume completely dominates over the statistical uncertainties on gas temperature and abundance. The structure of the shells appears clumpy in the X-ray images; however, there are too few counts to be able to determine adequately constrained physical properties for sub-regions of the shells. It is necessary to bear in mind in the discussion that follows that the density and pressure values we use for the shells are average values: the distribution of X-ray counts suggests that the surface brightness and hence the gas density in the shells is higher towards the centre of the radio source. We note that the contribution of X-ray binary emission to the surface brightness profile (Fig. 5) is unlikely to affect significantly our inferred densities, and any small effect will be in the direction of reducing the ISM density. The conclusions of Section 5.2 are therefore unaffected.

Since the external gas density and pressure in the environment of the radio source varies around the edge of the shells, we calculated the external density and pressure at several locations around the edge of the shells. Table 1 lists these properties at a distance of 10 arcsec from the nucleus of NGC 3801, which roughly corresponds to the midpoint of each shell. The uncertainty on the ISM density is dominated by including a systematic uncertainty due to the unconstrained metal abundance. In Section 5.2, we consider how the variation of shell and ISM properties may affect our results.

We also calculated the equipartition minimum internal pressure of the radio lobes, using measurements of the 1.4-GHz flux density for each lobe to normalize the synchrotron spectrum. We assumed a broken power-law electron distribution with initial electron energy index, δ, of 2.1, $\gamma_{\rm min} = 10$ and $\gamma_{\rm max} = 10^5$, and a break at $\gamma_{\rm break} = 10^3$, and modelled the lobes as spheres having volumes of 2.1×10^{10} pc^3 and 2.5×10^{10} pc^3 for the west and east lobes, respectively. The resulting pressures are given in Table 1.

The mass in each shell was also calculated in order to compare with the mass expected to have

been swept-up by the expanding radio lobes. We obtained a mass of $(5.3 - 7.7) \times 10^6$ $M_\odot$ for the West shell and $(2.0 - 6.1) \times 10^6$ $M_\odot$ for the East shell. The ISM mass swept up was calculated by modelling the radio lobes as expanding cones of 45° half-opening angle and integrating the best-fitting gas density distribution out to a distance of 2.1 kpc, which gives a total mass of $\sim 1.7 \times 10^7$ $M_\odot$, in fairly good agreement with the total shell mass. These calculations are therefore consistent with a scenario in which the shells consist of compressed material from the regions of the ISM through which the radio source has passed.

5.2. Dynamics of the lobe/ISM interaction

As shown in Table 1, the pressures in the hot shells of gas are higher than the minimum internal pressure of the radio lobes; since the shells and radio lobes must be in pressure balance, this suggests that the true radio lobe pressure is a factor of $\sim 4 - 6$ times the minimum value. Such a departure from minimum energy is generally observed in FRI radio galaxies for which external pressures can be measured (e.g. Morganti et al. 1988; Croston et al. 2003) and is also seen in the inner lobes of Centaurus A (e.g. Kraft et al. 2003). NGC 3801 is one of the few known FRI radio galaxies for which the *minimum* internal pressure is higher than the external pressure in the ISM (see Table 1); this is also the case for Cen A, and was one of the reasons we selected NGC 3801 as a *Chandra* target. The pressure in the X-ray shells of NGC 3801 (and by inference the true pressure in the radio lobes) is more than an order of magnitude higher than the local pressure in the interstellar medium.

The density contrast between the X-ray shells and the surrounding, undisturbed gas is slightly higher, but consistent with a value of ~ 4 for both the east and west shells, using the average shell density determined from the shell spectra, and the external gas density roughly halfway along the shells. This is the value expected if we are observing a strong shock for which the Rankine-Hugoniot jump conditions hold.

If we compare our value for the mean shell density with the external density at a distance of 5 arcsec, corresponding to the inner parts of the shells, the density contrast is ~ 3; however, as shown in Figs. 1 and 2, the brightest parts of the shell are in this region, so that the shell densities will be significantly higher than the mean value. The true density constrast in these inner regions is likely to be consistent with the expected value. The outer regions of the shell are fainter, so that the shell density is likely to be lower here. We conclude that it is plausible that the density contrast is in agreement with the value of 4 expected for a strong shock around the entire perimeter of the shells. Since the shell pressure should correspond to the internal radio lobe pressure, it should be uniform. This implies that the shell temperature at its outer edge should be considerably higher than the mean temperature in order to compensate for the lower gas density. Assuming a density contrast

of 4, we calculate a temperature of ~ 2.5 keV for the outer edge of the shell. The contribution of X-ray emission from this hotter region is not expected to be significant due to the lower density.

Assuming a density contrast of 4, we can use the Rankine-Hugoniot conditions to estimate the Mach number of the shock, as follows (Landau & Lifshitz 1990):

$$\mathcal{M} = \sqrt{\frac{4(\gamma+1)\frac{T_{shell}}{T_{ism}} + \gamma - 1}{2\gamma}} \tag{1}$$

which gives Mach numbers of 3.8 ± 1.3 and 3.2 ± 1.0 for the west and east shells respectively. The measured temperature increases are therefore consistent with the interpretation of both shells as originating in the boundary layer of a strong shock.

We also used a simple ram pressure balance calculation as a second means of estimating the shock advance speed as follows (using a density constrast of 4, consistent with the observed gas properties of the shell and ISM):

$$P_{shell} + \frac{1}{4}\rho_{ism} v_{ism}^2 = P_{ism} + \rho_{ism} v^2 \tag{2}$$

This leads to the following expression for $\mathcal{M}_{shell}$, the Mach number of the expanding shocked shell:

$$\mathcal{M}_{shell} = \frac{2\sqrt{5}}{3}\sqrt{\frac{P_{shell} - P_{ism}}{P_{ism}}} \tag{3}$$

which corresponds to $\mathcal{M}$ in the range $3.5 - 8.1$ for the West shell and in the range $2.9 - 6.8$ for the East shell, taking into account the uncertainty in the shell volume and the uncertainty in the ISM density due to the unconstrained abundance. These estimates are consistent with the values obtained from the measured temperature jump.

We conclude that we have indeed detected shells of strongly shocked gas around both radio lobes of NGC 3801, with Mach numbers of $3-8$, and shock conditions roughly consistent with the Rankine-Hugoniot jump conditions). If we assume that the radio source has expanded at $\mathcal{M} \sim 4$ throughout its lifetime, this gives a source age of $\sim 2 \times 10^6$ years, which is in good agreement with the upper limit estimated from spectral ageing in Section 4. The sound speed in the ISM is ~ 211 m s^{-1}, so that a Mach number of 4 corresponds to a lobe expansion speed of ~ 850 km s^{-1}.

There are a number of differences between the results we obtain for NGC 3801 and the shell in Cen A (Kraft et al. 2003). Firstly, the shell morphologies are different: in Cen A, only one shell is detected (although there may be some much fainter shell-like emission associated with the north-eastern lobe). In addition, the shell in Cen A is brightest at the outer edge of the radio lobe, whereas the NGC 3801 shells are brightest in the regions towards the nucleus. If lobe expansion is supersonic everywhere, the expansion of a uniform pressure radio lobe in an isothermal β-model

atmosphere should mean that the shock is weakest close to the nucleus; however, the higher density of the ISM in this region means that after compression its X-ray emission would nevertheless be expected to dominate. It is not clear why this is not observed in Cen A.

5.3. Implications for ISM energetics

The total thermal energy stored in the detected hot gas shells is calculated to be $(4.6 \pm 2.3) \times 10^{55}$ ergs and $(3.3 \pm 0.6) \times 10^{55}$ ergs for the West and East shells, respectively, or $\sim 8 \times 10^{55}$ ergs in total. Assuming a Mach number of 4, the kinetic energy of the shells is $(4.7 \pm 2.4) \times 10^{55}$ ergs per shell. Therefore, the total energy stored in the shocked shells is $(1.7 \pm 0.4) \times 10^{56}$ ergs. This is good agreement with the total work available from the radio lobes (assuming that the true internal lobe pressure is that of the shocked shells), $P_{int}V \sim 1.3 \times 10^{56}$ ergs. We calculate that the energy required to inflate both lobe cavities is $\sim 7 \times 10^{54}$ ergs, a factor of ~ 25 lower than the energy stored in the shells. Shock heating is therefore the dominant energy transfer mechanism during this stage of the radio source's evolution. Using the best-fitting gas density distribution, we find that this corresponds to the total thermal energy in the ISM within ~ 11 kpc (and roughly 25 percent of the total thermal energy within 30 kpc). The radio-source shock heating detected in NGC 3801 is therefore having a significant energetic impact on the host galaxy's ISM, and may provide enough energy to heat the gas sufficiently for the entire ISM to be expelled from the galaxy. We note that in addition, the internal energy of the radio source ($\sim 4 \times 10^{56}$ ergs) must eventually be transferred to the environment, although over a much longer timescale, and possibly at much larger distances.

Assuming a source age of 2×10^6 years (Section 4), this means that the radio source is putting work into the ISM at a rate of 3×10^{42} ergs s^{-1}, which should correspond to a significant fraction of the jet power. This is a plausible value, given that the most powerful FRI jets such as that in 3C 31 have jet powers of $\sim 10^{44}$ ergs s^{-1} (e.g. Laing & Bridle 2002). Our measurements of jet impact have therefore provided an independent means of estimating radio-jet power, which supports the more general validity of using jet-power arguments to estimate the energy input from radio galaxies into their environments. The rate of mechanical work that we calculate is roughly an order of magnitude higher than the X-ray luminosity of the obscured nuclear component (Section 3.3), so that the AGN must be more efficiently converting energy into jet production than into radiation.

To investigate the relationship between this energy output and accretion on the central black hole, we used the stellar velocity dispersion ($\sigma = 168$ km s^{-1}, Peletier et al. 1990) to estimate a black hole mass of $\log(M_{BH}/M_{\odot}) = 8.43$, using the relation of Tremaine et al. (2002). Assuming an efficiency of $\eta = 0.1$, the energy output we have measured from the radio source and shocked gas shells would require a total accreted mass of ~ 800 M$_{\odot}$, or an accretion rate of $\sim 4 \times 10^{-4}$ M$_{\odot}$ yr^{-1}, given the source age estimate above. For comparison, we calculate a Bondi accretion

rate of 2.5×10^{-3} $M_\odot$ yr^{-1} from the central hot gas, which suggests that Bondi accretion could be sufficient to provide the energy observed to be being transferred to the ISM from the central AGN by the radio lobes if the efficiency is relatively high (cf. Allen et al. 2006).

6. An extended, linear feature aligned with the radio jet

In addition to the bright shells discussed in the previous sections, the *Chandra* data also reveals a linear feature on scales of 10 – 20 kpc (shown in the 0.4 – 1 keV image of Fig. 7), which appears to be well-aligned with the inner radio jet axis. This feature has an extremely soft spectrum, well-fitted by a power law of photon index $\Gamma \sim 3.6$. The spectrum cannot be fitted by a thermal model with $kT > 0.1$ keV. There is no radio emission associated with this feature, nor does it appear to be associated with any optical or emission-line features. Although it has a similar orientation to one of the dust lanes, their position angles differ by ~ 15 degrees. The X-ray feature is not aligned with the chip axis, so that it is unlikely to be an instrumental artefact. We believe that the most plausible origin for this soft X-ray emission is a tidal or ram-pressure stripped tail, related to the merging/interactions of NGC 3801 with other nearby galaxies, including NGC 3802 to the north. The X-ray emission is therefore likely to be thermal emission from cooler, dense material stripped from the ISM of galaxies interacting with NGC 3801. Such emission could mimic the steep power-law spectrum we observe.

It could be argued that the presence of X-ray features produced by tidal debris might suggest a tidal origin for the features coincident with the radio lobes. It is not possible to rule out such a model definitively; however, the strong morphological agreement between radio and X-ray structure, the significant differences in the spectral properties of the shell features and tidal tails, and the fact that we know the radio lobes to be overpressured and hence supersonically expanding, all support our interpretation of the radio-related X-ray emission as shocked gas.

7. Relationship between the host galaxy and radio-source properties

Both Cen A and NGC 3801 possess strong evidence for a recent merger with a gas-rich galaxy, which may be more typical of FRII host galaxies compared to the hosts of more powerful FRIs (e.g. Heckman et al. 1986; Colina & DeJuan 1995). It is therefore interesting to consider the relationship between their merger history, radio outbursts, and their effects on the ISM as revealed by *Chandra*. NGC 3801 and Cen A have another feature in common, which may be related to their merger history: they are the only two FRI radio galaxies that we know of whose nuclear spectra require the presence of a high absorbing column ($N_H \gtrsim 5 \times 10^{22}$), so that they are the only known

FRIs that possess any evidence for the torus often found in powerful, high-excitation (FRII) radio galaxies and quasars (Hardcastle et al. 2006). Although we cannot draw strong conclusions from two objects, it is interesting to speculate that these two sources may be fuelled in the same way as FRII radio galaxies. It is possible that these two radio galaxies represent a class of post-merger system in which cold gas is driven into the inner regions to fuel the central AGN and trigger a radio outburst. On the other hand, the presence of fainter larger-scale radio structure surrounding the inner lobes of Cen A means that in that case at least, the young central radio source does not represent the first or only radio outburst. Our radio data show no evidence for previous generations of radio activity in NGC 3801.

Radio-loud AGN that are fuelled by the accretion of cold gas from recent merger events are not self-regulating in the same way as AGN fuelled by direct accretion of the hot phase of the ISM (e.g. by Bondi accretion: Allen et al. 2006), since the AGN impact on the hot phase does not affect the accretion rate of cold material. In these systems, therefore, the long-term effects of AGN energy input may be particularly extreme.

8. Conclusions

We have detected shells of shocked gas surrounding both radio lobes of NGC 3801. We infer Mach numbers of $3 - 6$ for the shock advance speeds, so that our results correspond to the second detection of strong shocks associated with a low-power radio galaxy. The total energy stored in the shock-heated shells represents a large fraction of the total thermal energy of the host galaxy, so that the long-term effects of the NGC 3801 outburst are likely to be dramatic. This is the first case where the total energetic impact of a radio galaxy on its environment can be directly measured, and suggests that the energetic contribution of an early supersonic phase is likely to be important in low-power radio galaxies. The energy stored in the shocked gas is 25 times the PdV work required to inflate the radio-lobe cavities, so that during this phase of its evolution, shock heating is the dominant mechanism of energy transfer from NGC 3801 to its environment.

We gratefully acknowledge support from the Royal Society (research fellowship for MJH). This work was partially supported by NASA grant GO6-7095X. The National Radio Astronomy Observatory is a facility of the National Science Foundation operated under cooperative agreement by Associated Universities.

REFERENCES

Allen, S. W., Dunn, R. J. H., Fabian, A. C., Taylor, G. B. & Reynolds, C. S. 2006, *MNRAS*, submitted, astro-ph/0602549

Best, P. N. 2004, *MNRAS*, 351, 70

Burstein, D., Davies, R. L., Dressler, A., Faber,7 S. M., Stone, R. P. S., Lynden-Bell, D., Terlevich, & R. J. Wegner, G. 1987, *ApJS*, 60, 601

Colina, L. & de Juan, L. 1995 *ApJ*, 448, 558

Croston, J. H., Hardcastle, M. J., Birkinshaw, M. & Worrall, D. M. 2003, *MNRAS*, 346, 1041

Croston, J.H., Hardcastle, M.J., Harris, D.E., Belsole, E., Birkinshaw, M., & Worrall, D.M. 2005, *ApJ*, 626, 733

Das, M., Vogel, S. N., Verdoes Kleijn, G. A., O'Dea, C. P. & Baum, S. A. 2005, *ApJ*, 629, 757

Dickey, J. M. & Lockman, F. J. 1990, *ARA&A*, 28, 215

Evans, D. A., Kraft, R. P., Worrall, D. M., Hardcastle, M. J., Jones, C., Forman, W. R. & Murray, S. S. 2004 *ApJ*,612, 786

Evans, D. A., Worrall, D. M., Hardcastle, M. J., Kraft, R. P. & Birkinshaw, M. 2006, *ApJ*, 642, 96

Fabian, A. C., Sanders, J. S., Allen, S. W., Crawford, C. S., Iwasawa, K., Johnstone, R. M., Schmidt, R. W. & Taylor, G. B. 2003, *MNRAS*, 344,, L43

Fanaroff, B. L. & Riley, J. M. 1974, *MNRAS*, 167, 31P

Hardcastle, M. J., Evans, D. A. & Croston, J. H. 2006, *MNRAS*, in press (astro-ph/0603090)

Heckman, T. M., Smith, E. P., Baum, S. A., van Breugel, W. J. M., Miley, G. K., Illingworth, G. D., Bothun, G. D. & Balick, B. 1989 *ApJ*,311, 526

Heinz, S.,Reynolds, C. S. & Begelman, M. C. 1998, *ApJ*, 501, 126

Kraft, R. P., Vázquez, S. E., Forman, W. R., Jones, C., Murray, S. S., Hardcastle, M. J., Worrall, D. M. & Churazov, E. 2003, *ApJ*, 592, 129

Laing, R. A. & Bridle, A. H. 2002, *MNRAS*, 336, 1161

Landau, L. D. & Lifschitz, E. M. 1990, *Fluid Mechanics, Vol 6*, (Oxford, Butterworth-Heinemann)

Lu, N. Y., Hoffman, G. L., Groff, T., Roos, T. & Lamphier, C. 1993, *ApJS*, 88, 383

Morganti, R., Fanti, R., Gioia, I. M., Harris, D. E., Parma, P. & de Ruiter, H. 1988, *A&A*, 189, 11

McNamara, B. R., Nulsen, P. E. J., Wise, M. W., Rafferty, D. A., Carilli, C., Sarazin, C. L., & Blanton, E. L. 2005, *Nature*, 433, 45

O'Sullivan, E., Ponman, T. J. & Collins, R. S. 2003, *AJ*, 340, 1375

Peletier, R. F., Davies, R. L., Illingworth, G. D., Davis, L. E. & Cawson, M. 1990, *AJ*, 100, 1091

Tremaine, S., Gebhardt, K., Bender, R., Bower, G., Dressler, A., Faber, S. M., Filippenko, A. V., Green, R., Grillmair, C. ,Ho, L. C., Kormendy, J., Lauer, T. R., Magorrian, J., Pinkney, J. & Richstone, D. 2002, *ApJ*, 574, 740

Verdoes Kleijn, G. A., Baum, S. A., de Zeeuw, P. T. & O'Dea, C. P. 1999, *AJ*, 118, 2592

Worrall, D. M., Birkinshaw, M. & Hardcastle, M. J. 2001, *MNRAS*, 326, L7

Young, A. J., Wilson, A. S. & Mundell, C. G. 2002, *ApJ*, 579, 560

Zombeck, M. V. 1990, Handbook of Space Astronomy and Astrophysics, CUP.

Table 1. Temperature, density and pressure of shells and surrounding ISM. The ISM values correspond to a distance of 10 arcsec from the nucleus of NGC 3801, which is roughly midway along the shells. For the shell densities and pressures we quote a range corresponding to the two volume estimates described in Section 5.1, and for the ISM density and pressure we quote in parentheses the range corresponding to the range in abundance and temperature as described in Section 3.2. The shell/ISM ratios for density and pressure are for an ISM abundance of 0.4 times solar.

Feature	West shell	East shell
kT_{shell} (keV)	$1.0^{+0.4}_{-0.3}$	$0.71^{+0.08}_{-0.04}$
kT_{ISM} (keV)	$0.23^{+0.21}_{-0.09}$	$0.23^{+0.21}_{-0.09}$
$n_{e,shell}$ (cm^{-3})	$(2.0-3.0)\times10^{-2}$	$(2.0-3.0)\times10^{-2}$
$n_{e,ISM}$ (cm^{-3})	$4.6(3.8-9.2)\times10^{-3}$	$4.6(3.8-9.2)\times10^{-3}$
n_{shell}/n_{ism}	$4.3-6.5$	$4.3-6.5$
P_{shell} (Pa)	$(5.9-8.9)\times10^{-12}$	$(4.2-6.4)\times10^{-12}$
P_{ISM}(Pa)	$3.8(2.9-8.9)\times10^{-13}$	$3.8(2.9-8.9)\times10^{-13}$
P_{int}(Pa)	1.1×10^{-12}	1.3×10^{-12}
P_{shell}/P_{ism}	$15-23$	$11-17$
P_{int}/P_{ism}	2.9	3.4

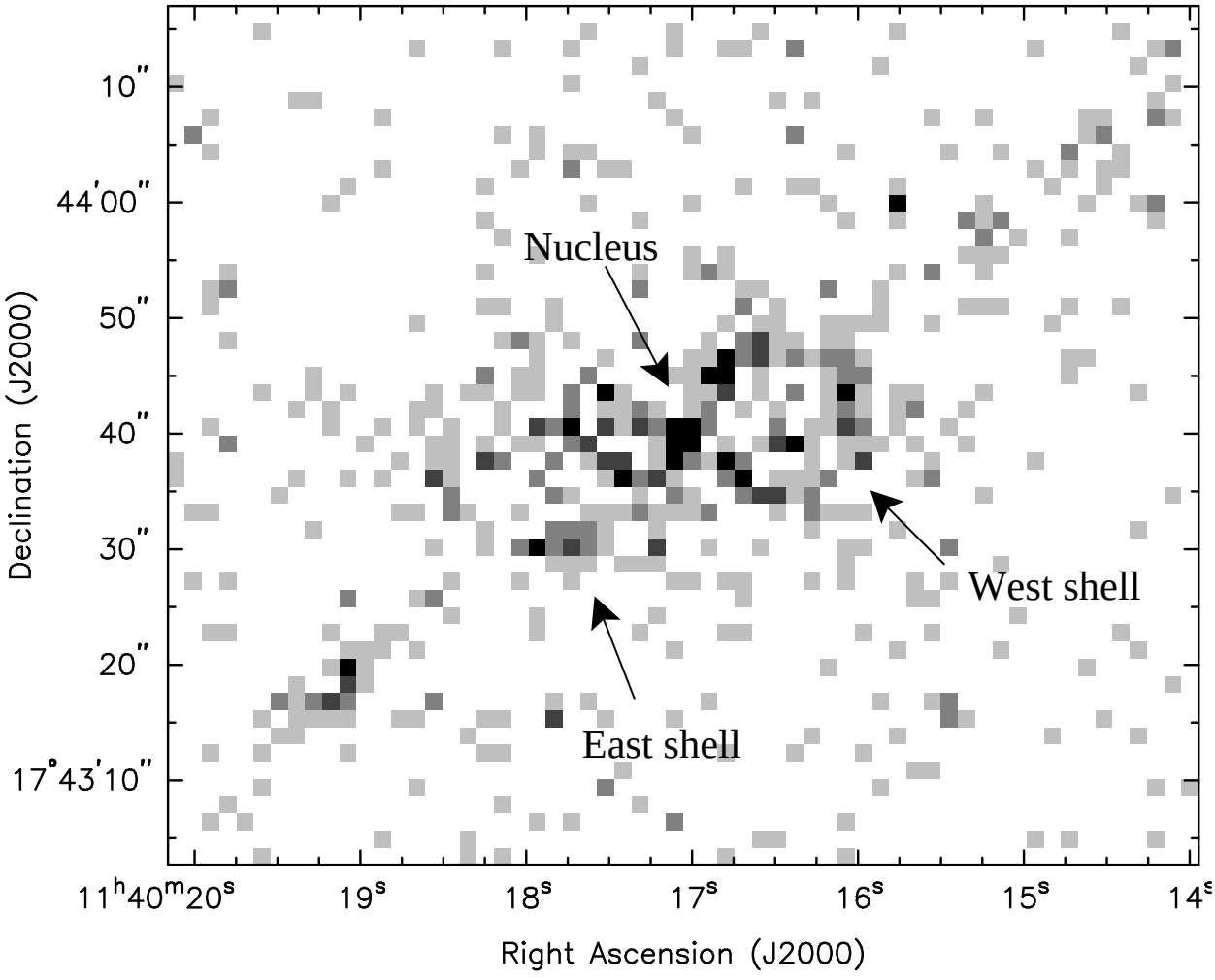

Fig. 1.— A 0.5 – 2 keV image of the *Chandra* data, binned by a factor of 3, revealing the symmetrical shell features associated with NGC 3801

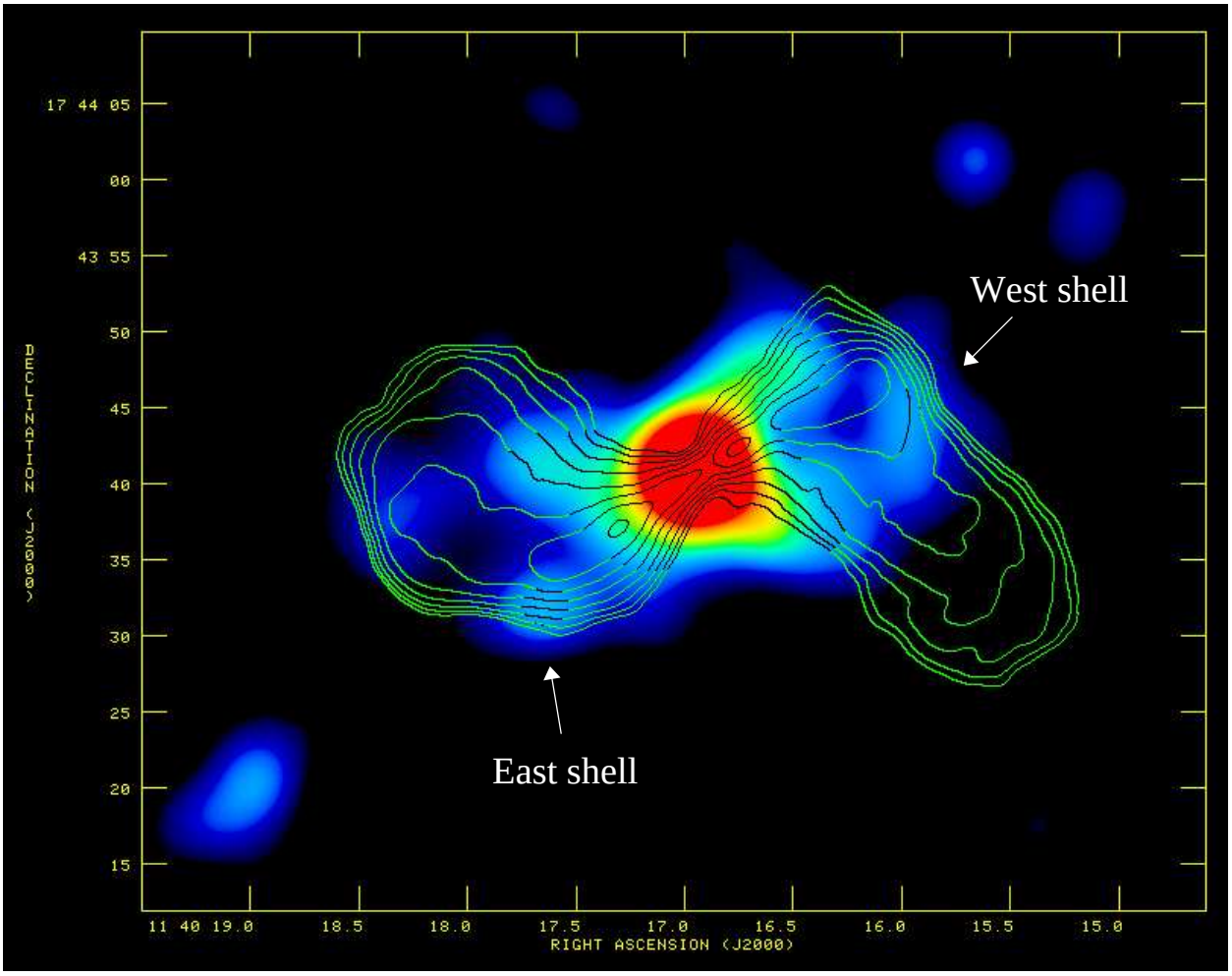

Fig. 2.— Gaussian smoothed ($\sigma = 1.97$ arcsec) 0.5 – 5 keV image of the *Chandra* data, with 1.4-GHz radio contours overlaid to illustrate the relationship between the X-ray shells and radio morphology.

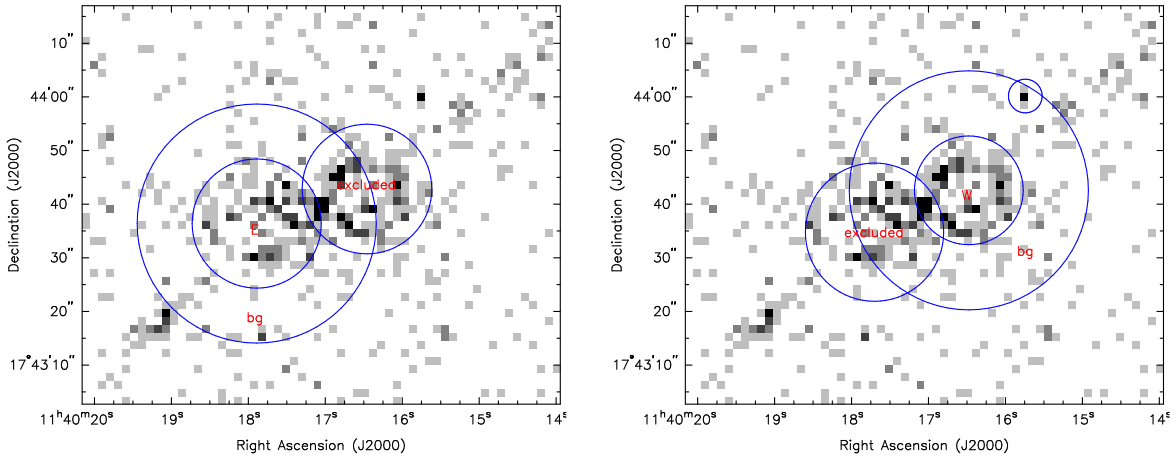

Fig. 3.— The source and background regions used for spectral analysis of the X-ray shell emission.

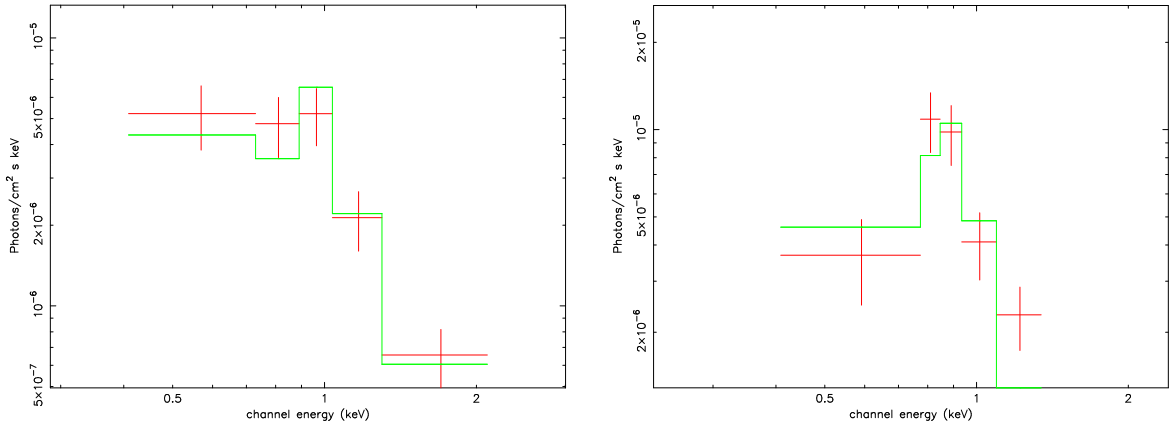

Fig. 4.— The spectra for the west and east lobe-related regions of X-ray emission with best-fitting *mekal* models as described in the text.

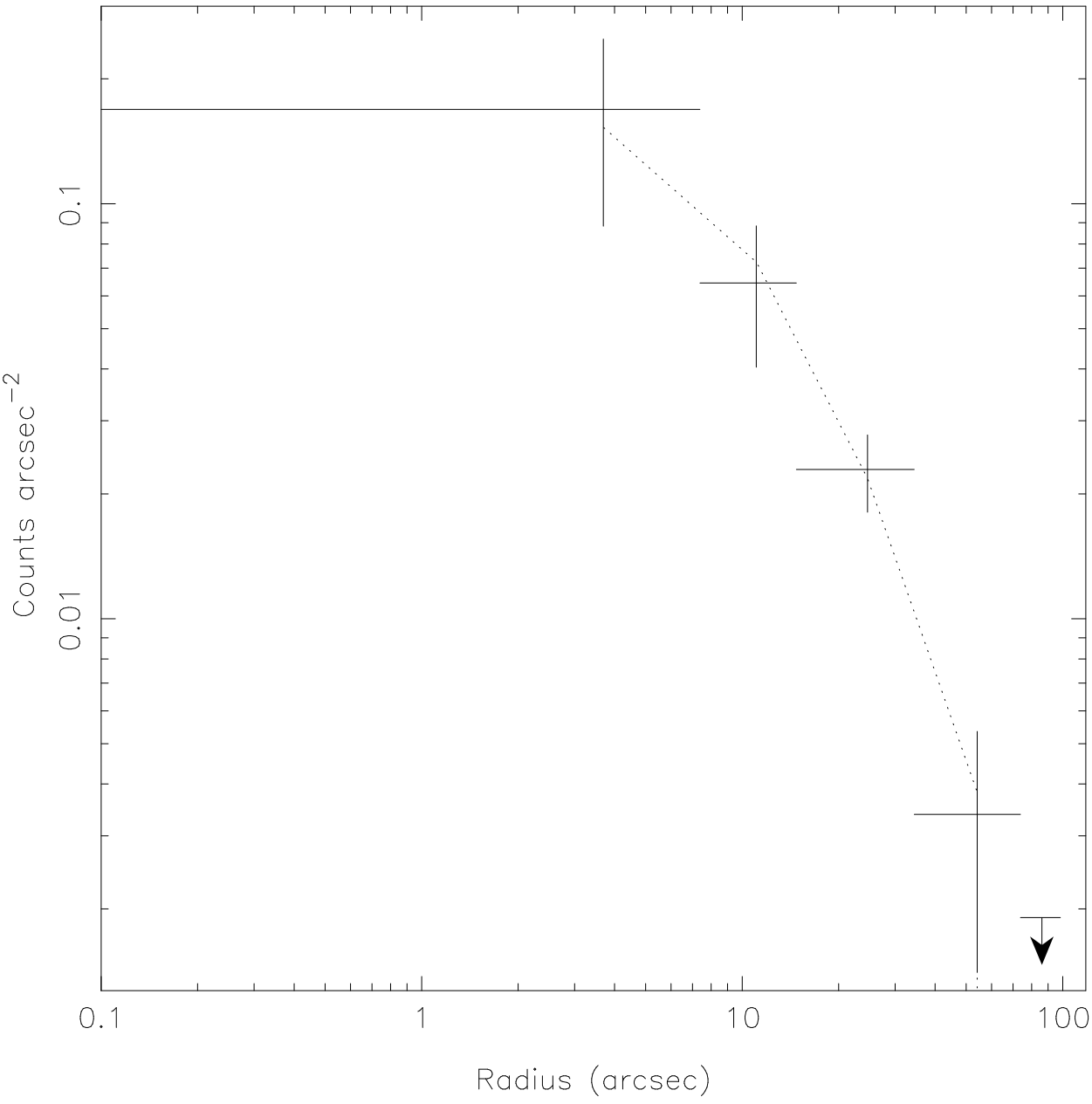

Fig. 5.— Background-subtracted surface brightness profile extracted from the 0.5 – 2 keV *Chandra* events list with best-fitting β model having $\beta = 0.45$ and $r_c = 7$ arcsec.

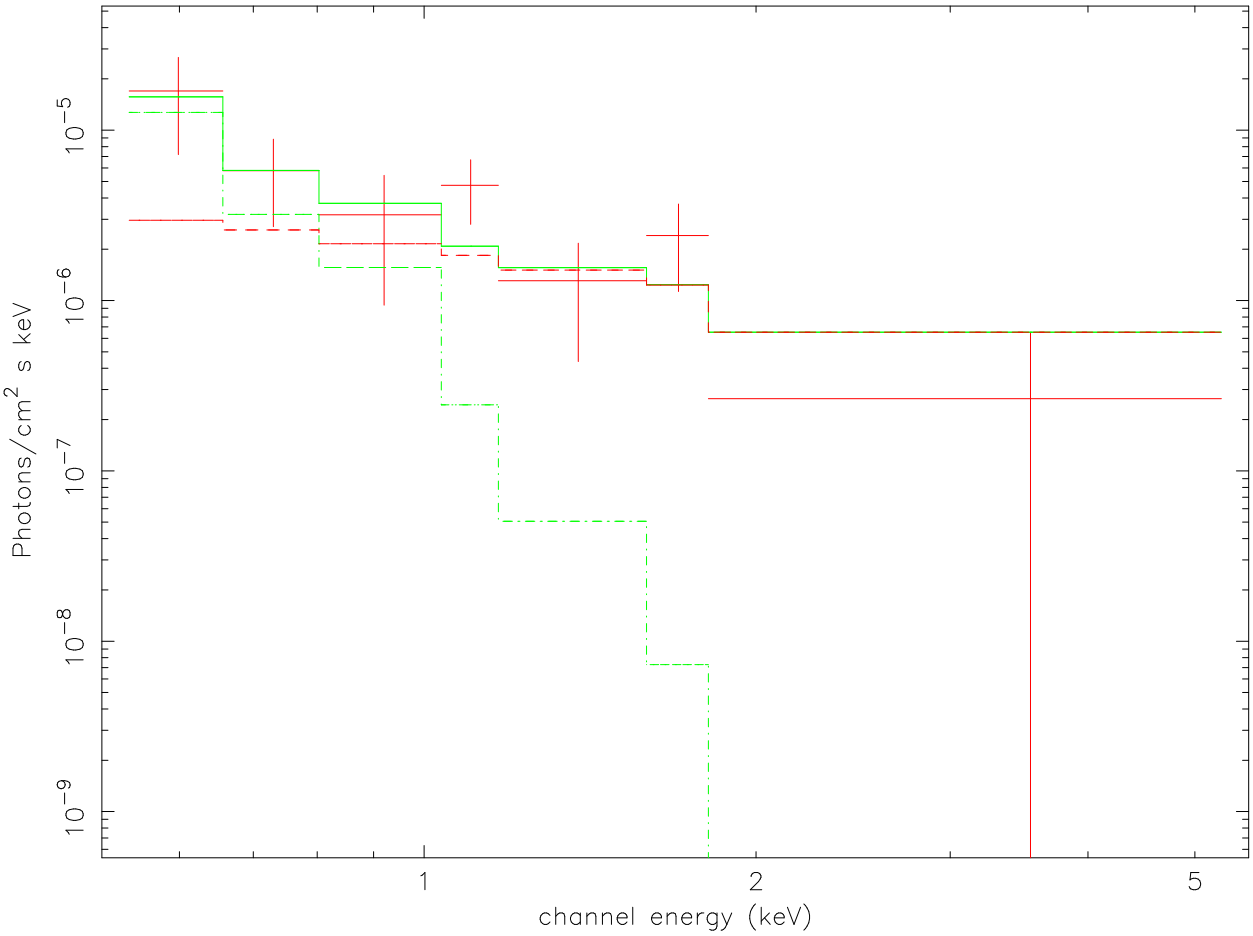

Fig. 6.— The spectrum of the ISM with best-fitting *mekal* plus power-law model, as discussed in detail in the text.

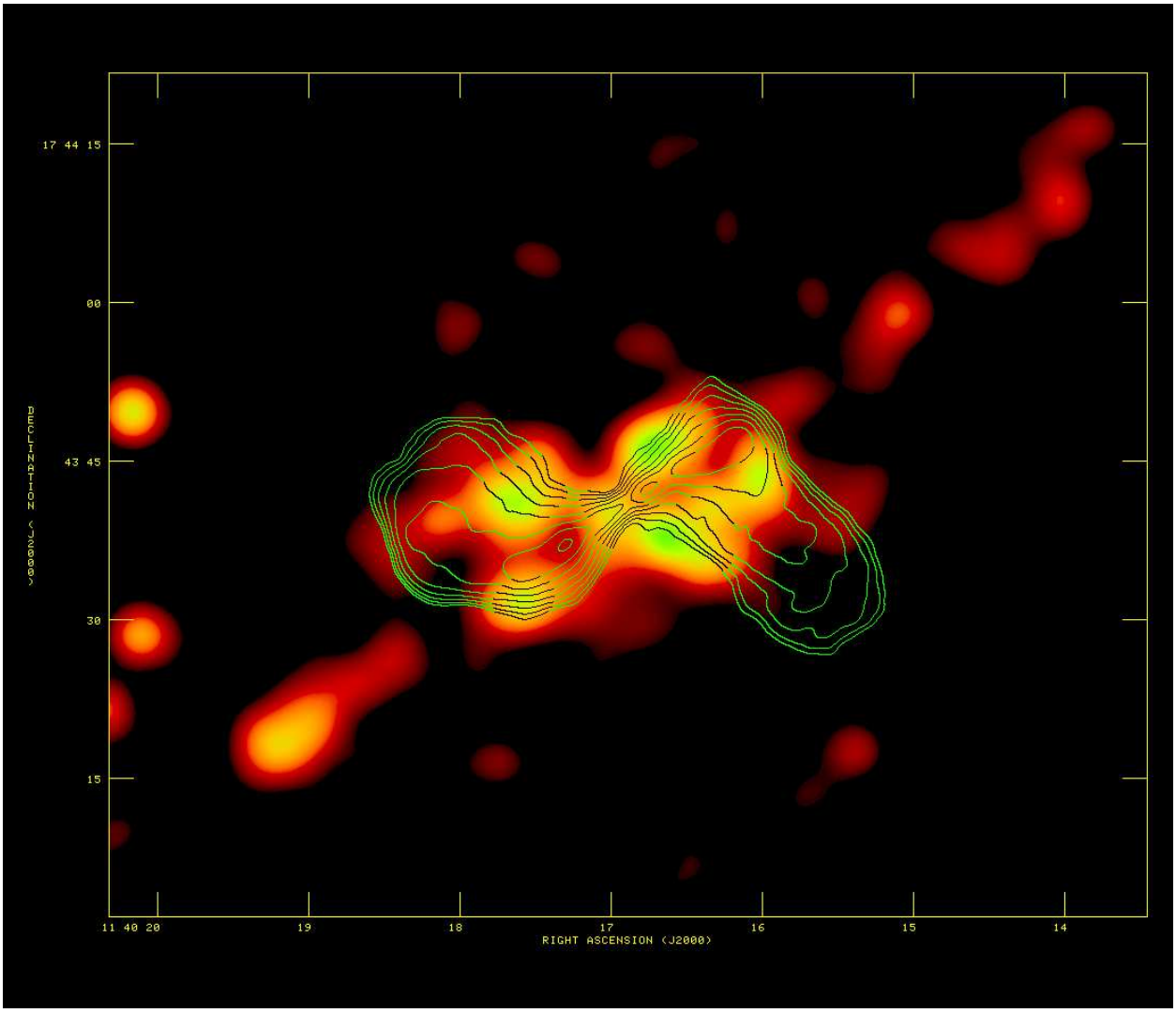

Fig. 7.— Gaussian smoothed ($\sigma = 1.97$ arcsec) 0.4 – 1 keV image of the *Chandra* data, with 1.4-GHz radio contours overlaid, indicating the soft, extended feature aligned with the jet axis.

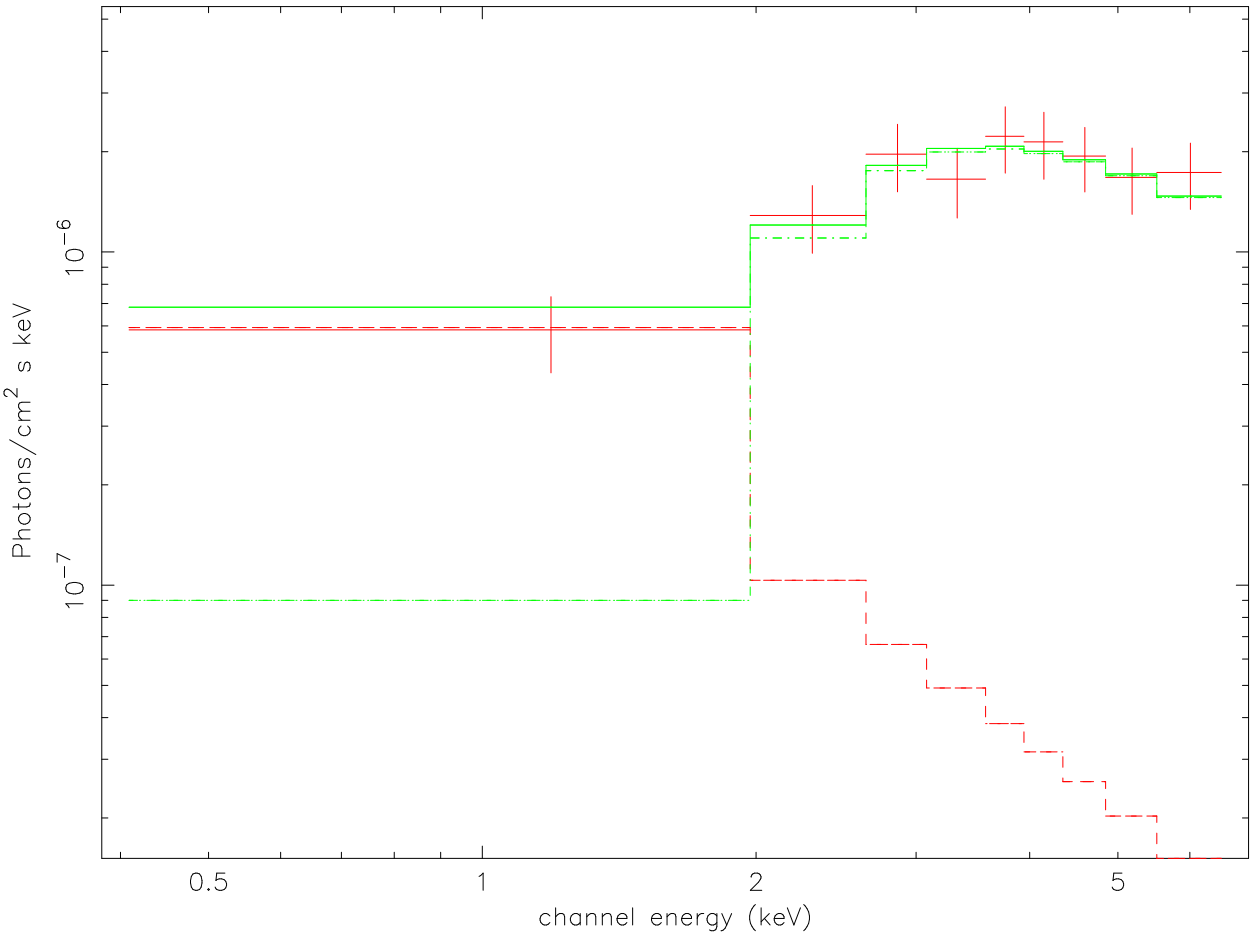

Fig. 8.— Core spectrum (in the energy range 0.4 - 7 keV) with best-fitting model as described in the text.